Inorg. Chem. **2009**, *48*, 2028−2042

Inorganic Chemistry
Article

Spin-Frustrated Complex, $[Fe^{II}Fe^{III}(\textit{trans}\text{-1,4-cyclohexanedicarboxylate})_{1.5}]_\infty$: Interplay between Single-Chain Magnetic Behavior and Magnetic Ordering

Yan-Zhen Zheng,[†] Wei Xue,[†] Wei-Xiong Zhang,[†] Ming-Liang Tong,[†] Xiao-Ming Chen,[*,†] Fernande Grandjean,[‡] Gary J. Long,[*,§] Seik-Weng Ng,[||] Pierre Panissod,[⊥] and Marc Drillon[⊥]

Laboratory of Bioinorganic and Synthetic Chemistry, School of Chemistry & Chemical Engineering, Sun Yat-Sen University, Guangzhou 510275, China, Department of Physics, B5, University of Liège, B-4000 Sart-Tilman, Belgium, Department of Chemistry, Missouri University of Science and Technology, University of Missouri-Rolla, Rolla, Missouri 65409-0010, Department of Chemistry, University of Malaya, 50603 Kuala Lumpur, Malaysia, and Institut de Physique et Chimie des Matériaux de Strasbourg, 23 rue du Loess, Unité Mixte de Recherches Centre National de la Recherche Scientifique-Université Louis Pasteur, F-67034 Strasbourg, France

Received October 8, 2008

A three-dimensional mixed-valent iron(II,III) *trans*-1,4-cyclohexanedicarboxylate, 1,4-chdc, coordination polymer, $[Fe^{II}Fe^{III}(\mu_4\text{-O})(1,4\text{-chdc})_{1.5}]_\infty$, **1**, has been synthesized hydrothermally by mixing iron powder and 1,4-chdcH$_2$ and investigated by X-ray diffraction, dc and ac magnetic susceptibility, and iron-57 Mössbauer spectroscopy over a wide range of temperatures. Single-crystal X-ray diffraction studies of **1** at 90(2), 293(2), and 473(2) K reveal a tetrahedral $[Fe^{II}_2(\mu_4\text{-O})Fe^{III}_2(\mu_4\text{-O})]^{6+}$ mixed-spin-chain structure with no change in the $P\bar{1}$ space group but with subtle changes in the Fe−O and Fe···Fe distances with increasing temperature. These changes are associated with the electron delocalization observed by Mössbauer spectroscopy above 225 K. Magnetic studies reveal three different magnetic regimes in **1** between 2 and 320 K. Above 36 K **1** is a one-dimensional ferrimagnetic-like complex with frustration arising from competing exchange interactions between the iron(II) and iron(III) ions in the chains. Between 36 and 25 K the interchain interactions are non-negligible and **1** undergoes three-dimensional ordering at 32.16 K but with some residual fluctuations. Below 25 K the residual fluctuations slow and eventually freeze below 15 K; the small net moment of 0.22 μ_B per mole of **1** observed below 15 K may be attributed to a non-collinear or canted spin structure of the spins of the four iron ions in the $[Fe^{II}_2(\mu_4\text{-O})Fe^{III}_2(\mu_4\text{-O})]^{6+}$ chains. Below 32 K the Mössbauer spectra of **1** exhibit sharp sextets for both the iron(III) and iron(II) ions and are consistent with either a static long-range or a short-range magnetic ground state or a slow relaxation between two canted magnetic states that are indistinguishable at the observed spectral resolution. The 85 and 155 K spectra reveal no electron delocalization and correspond solely to fixed valence iron(II) and iron(III). Between 225 and 310 K the spectra reveal the onset of electron delocalization such that, at 295 to 310 K, 25, 25, and 50% of the iron in **1** is present as iron(II), iron(III), and iron(II/III) ions, respectively. The absence of any spectral line broadening associated with this electron delocalization and the coexistence of four doublets between 225 and 310 K indicate that the delocalization occurs through electron tunneling via vibronic coupling. The sudden increase in the tunneling rate beginning above about 260 K and the presence of a cusp in the magnetic susceptibility centered at about 275 K strongly suggest the existence of a charge order/disorder transition whose nature and order are discussed.

Introduction

The presence of magnetic spin frustration has led to interest in one-dimensional quantum spin complexes. The most common structural features of such complexes are a triangular, square, or tetrahedral arrangement of spins interacting antiferromagnetically.[1,2] Over the past decade, triangle-based

---

[*] To whom correspondence should be addressed. E-mail: cxm@mail.sysu.edu.cn (X.-M.C.), glong@mst.edu (G.J.L.). Fax: (+)86 20 8411-2245 (X.-M.C.), (573) 341-6033 (G.J.L.).

[†] Sun Yat-Sen University.

[‡] University of Liège.

[§] University of Missouri-Rolla.

[||] University of Malaya.

[⊥] Institut de Physique et Chimie des Matériaux de Strasbourg.

(1) (a) Mikeska, H.-J.; Kolezhuk, A. K. In *Quantum Magnetism*; Schollwöck, U., Richter, J., Farnell, D. J. J., Bishop, R. F., Eds.; Springer: Berlin, 2004; pp 1−83. (b) Lecheminant, P. In *Frustrated Spin Systems*; Diep, H. P., Ed.; World Scientific Publishing: Singapore, 2004, pp 307−366. (c) Georges, R.; Borrás-Almenar, J. J.; Coronado, E.; Curély, J.; Drillon, M. In *Magnetism: Molecules to Materials I*; Miller, J. S., Drillon, M., Eds.; Wiley-VCH: New York, 2001, pp 1−47.

10.1021/ic8019155 CCC: $40.75

frustrated chains, such as the sawtooth,[3a] corner-sharing triangular,[3b] zigzag,[3c] diamond,[3d] and orthogonal-dimer chains[3e] and the square-based frustrated spin-ladders, see Supporting Information, Scheme S1, have been investigated both experimentally and theoretically. In contrast, one-dimensional corner-sharing or edge-sharing tetrahedral-based chains have been less well studied, especially from an experimental point of view.[4]

The current interest in the tetrahedral-based chains has been stimulated by the discovery of both a "spin-ice" pyrochlore structure,[5] a structure in which magnetic rare-earth ions form a lattice of corner-sharing and edge-sharing tetrahedral chains that exhibit diagonal spin exchange, an exchange that is equivalent to the diagonal spin-exchange interactions found in a two-legged spin-ladder. Therefore, model compounds of one to three-dimensional networks of frustrated tetrahedra, with variable intertetrahedral exchange coupling, are very useful in investigating the exotic behavior of a spin-ice or a spin-ladder magnetic complex.[4,5]

At this time rather little is known, particularly from an experimental point of view, about the role of frustration in the so-called mixed-spin-chains constructed with two or more different spin sites regularly arranged in a lattice.[6,7] Theoretically such systems are paradigmatic examples of strong magnetic correlation with different types of excitations, that is, they exhibit both gapless and gapped excitations at relatively low-energy.[6,7] However, the preparation of genuine spin-chain compounds possessing both frustrated topology and mixed spins is still a challenge, and their paucity hampers the investigation of their predicted exotic magnetic behavior. In this context, mixed-valence complexes[8] are useful for preparing frustrated mixed spin complexes,[9] first, because they are naturally mixed-spin and, second, because they form complexes with triangular or tetrahedral clusters that can share delocalized electrons. One recently discovered example of a complex with frustrated mixed spins is the mixed-valence iron sulfate possessing a sawtooth Fe−F chain.[9a] Interestingly, in contrast to the regular Kagomé structures formed by other mixed-valence iron sulfates, this sawtooth Fe−F chain half-Kagomé structure exhibits no clear evidence of magnetic spin frustration.

Recently, we have used homonuclear $M_3[\mu_3\text{-O(H)}]$ clusters, where M is Fe^{III}, Fe^{II}, Co^{II}, or Co^{III}, to generate several triangular frustrated lattices, such as the Δ-chain,[10a] Kagomé,[10b] "star,"[10c] and related lattices.[10d,e] Moreover, we have also assembled Ising ferromagnetic Co^{II}−O chains[10f] and Fe^{II}−O chains[10g] into two-dimensional networks by using the "magnetically-inert" σ-bonded *trans*-1,2-cyclohexanedicarboxylate and the half σ-bonded 2-(pyridin-3-yloxy)-acetate ligands, respectively. We are now able to combine these two strategies to construct $[Fe^{II}_2(\mu_4\text{-O})Fe^{III}_2(\mu_4\text{-O})]^{6+}$ based chains with mixed-valence iron and, thus, with mixed spins, in a carboxylate-bridged three-dimensional network. This has been accomplished by using a bridging *trans*-1,4-cyclohexanedicarboxylate ligand to form, $[Fe^{II}Fe^{III}(\mu_4\text{-O})(\textit{trans}\text{-1,4-cyclohexanedicarboxylate})_{1.5}]_\infty$, herein referred to as $[Fe^{II}Fe^{III}(\mu_4\text{-O})(1,4\text{-chdc})_{1.5}]_\infty$, **1**, a linear-chain polymer that exhibits extensive electronic delocalization between 225 and 310 K, single-chain magnetism above 36 K, and three-dimension magnetic order below 32.16 K.

Experimental Section

Materials and Physical Measurements. Commercially available reagents have been used as received without further purification. The C, H, and N microanalyses have been carried out with an Elementar Vario-EL CHNS elemental analyzer. The FT-IR spectra have been obtained in KBr between 4000 and 400 cm^{-1} on a Bio-Rad FTS-7 spectrometer. Powder X-ray diffraction measurements were obtained with a Rigaku D/max-IIIA diffractometer by using Cu K_α, $\lambda = 1.54056$ Å, radiation and a scan rate of 2°/min over a 2θ range of 4 to 55°. A standard X-ray diffraction pattern has been generated by using the Cambridge Mercury 1.4.2 software.

Magnetic susceptibility measurements on **1** have been carried out with a Quantum Design MPMS-XL7 SQUID magnetometer upon cooling from 320 to 2 K in a 0.010 T applied field. Further, the direct current (dc) magnetization has been measured between 2 and 70 K in applied fields of 0.005 to 5 T and between applied fields of ±7 T between 7.5 and 12 K. Alternating current (ac)

---

(2) (a) Ramirez, A. P. In *Handbook of Magnetic Materials*; Buschow, K. H. J., Ed.; Elsevier: Amsterdam, 2001; Vol 13, pp 423−520. (b) Greedan, J. E. *J. Mater. Chem.* **2001**, *11*, 37. (c) Harrison, A. *J. Phys.: Condens. Matter* **2004**, *16*, S553. (d) Ramirez, A. P. *MRS Bull.* **2005**, *30*, 447. (e) Greedan, J. E. *J. Alloys Compd.* **2006**, *408−412*, 444.

(3) (a) Chandra, V. R.; Sen, D.; Ivanov, N. B.; Richter, J. *Phys. Rev. B* **2004**, *69*, 214406. (b) Gutschke, S. O. H.; Price, D. J.; Powell, A. K.; Wood, P. T. *Angew. Chem., Int. Ed.* **2001**, *40*, 1920. (c) Maeshima, N.; Hagiwara, M.; Narumi, Y.; Kindo, K.; Kobayashi, T. C.; Okunishi, K. *J. Phys.: Condens. Matter* **2003**, *15*, 3607. (d) Kikuchi, H.; Fuji, Y.; Chiba, M.; Mitsudo, S.; Idehara, T.; Tonegawa, T.; Okamoto, K.; Sakai, T.; Kuwai, T.; Ohta, H. *Phys. Rev. Lett.* **2005**, *94*, 227201. (e) Schulenburg, J.; Richter, J. *Phys. Rev. B* **2002**, *66*, 134419.

(4) (a) Brenig, W.; Becker, K. W. *Phys. Rev. B* **2001**, *64*, 214413. (b) Totsuka, K.; Mikeska, H.-J. *Phys. Rev. B* **2002**, *66*, 054435. (c) Brenig, W. *Phys. Rev. B* **2003**, *67*, 064402. (d) Rojas, O.; Corrêa Silva, E. V.; de Souza, S. M.; Thomaz, M. T. *Phys. Rev. B* **2004**, *69*, 134405. (e) Arlegoa, M.; Brenig, W. *Eur. Phys. J. B* **2006**, *53*, 193. (f) Chen, S.; Wang, Y.; Ning, W. Q.; Wu, C.; Lin, H. Q. *Phys. Rev. B* **2006**, *74*, 174424.

(5) Bramwell, S. T.; Gingras, M. J. P.; Holdsworth, P. C. W. In *Frustrated Spin Systems*; Diep, H. P., Ed.; World Scientific Publishing: Singapore, 2004; Vol. 36, pp 7−456. (b) Wang, R. F.; Nisoli, C.; Freitas, R. S.; Li, J.; McConville, W.; Cooley, B. J.; Lund, M. S.; Samarth, N.; Leighton, C.; Crespi, V. H.; Schiffer, P. *Nature* **2006**, *439*, 303.

(6) (a) Ivanov, N. B.; Richter, J. *Phys. Rev. B* **2004**, *69*, 214420. (b) Ivanov, N. B.; Richter, J. *Phys. Rev. B* **2006**, *73*, 132407. (c) Ivanov, N. B.; Richter, J.; Schollwöck, U. *Phys. Rev. B* **1998**, *58*, 14456.

(7) (a) Koga, A.; Kumada, S.; Kawakami, N.; Fukui, T. *J. Phys. Soc. Jpn.* **1998**, *67*, 622. (b) Trumper, A. E.; Gazza, C. *Phys. Rev. B* **2001**, *64*, 134408. (c) Fukui, T.; Kawakami, N. *Phys. Rev. B* **1998**, *57*, 398. (d) Tian, G.-S.; Lin, H.-Q. *Phys. Rev. B* **2004**, *70*, 104412. (e) Chen, S.; Wang, L.; Wang, Y. P. *Eur. Phys. J. B* **2007**, *57*, 265.

(8) Borrás-Almenar, J. J.; Clemente-Juan, J. M.; Coronado, E.; Palii, A.; Tsukerblat, B. S. In *Magnetism: Molecules to Materials, I*; Miller, J. S., Drillon, M., Eds.; Wiley-VCH: New York, 2001; pp 155−208.

(9) (a) Behera, J. N.; Rao, C. N. R. *Chem. Asian J.* **2006**, *1*, 742. (b) Paul, G.; Choudhury, A.; Sampathkumaran, E. V.; Rao, C. N. R. *Angew. Chem., Int. Ed.* **2002**, *41*, 4297.

(10) (a) Cheng, X.-N.; Zhang, W.-X.; Zheng, Y.-Z.; Chen, X.-M. *J. Chem. Soc., Chem. Commun.* **2006**, 3603. (b) Zheng, Y.-Z.; Tong, M.-L.; Zhang, W.-X.; Chen, X.-M. *J. Chem. Soc., Chem. Commun.* **2006**, 165. (c) Zheng, Y.-Z.; Tong, M.-L.; Xue, W.; Zhang, W.-X.; Chen, X.-M.; Grandjean, F.; Long, G. J. *Angew. Chem., Int. Ed.* **2007**, *46*, 6076. (d) Zeng, M.-H.; Zhang, W.-X.; Chen, X.-M. *J. Chem. Soc., Dalton Trans.* **2006**, 5294. (e) Zhang, X.-M.; Zheng, Y.-Z.; Li, C.-R.; Zhang, W.-X.; Chen, X.-M. *Cryst. Growth Des.* **2007**, *7*, 980. (f) Zheng, Y.-Z.; Tong, M.-L.; Zhang, W.-X.; Chen, X.-M. *Angew. Chem., Int. Ed.* **2006**, *45*, 6310. (g) Zheng, Y.-Z.; Tong, M.-L.; Xue, W.; Zhang, W.-X.; Chen, X.-M.; Grandjean, F.; Long, G. J. *Inorg. Chem.* **2008**, *47*, 4077.

Table 1. Crystallographic Data and Structural Refinements for **1**

T (K)	90(2)	293(2)	473(2)
formula	$C_{12}H_{15}Fe_2O_7$	$C_{12}H_{15}Fe_2O_7$	$C_{12}H_{15}Fe_2O_7$
formula weight (g/mol)	382.94	382.94	382.94
space group	$P\bar{1}$ (No. 2)	$P\bar{1}$ (No. 2)	$P\bar{1}$ (No. 2)
a (Å)	5.0776(3)	5.0752(4)	5.097(2)
b (Å)	12.0535(7)	12.0881(8)	12.134(8)
c (Å)	12.4580(7)	12.3513(9)	12.43(1)
α (deg)	119.772(1)	118.763(1)	118.97(8)
β (deg)	94.367(1)	93.885(1)	93.42(5)
γ (deg)	90.055(1)	90.690(1)	91.15(4)
V (Å^3)	659.24(7)	661.86(8)	670.1(8)
Z	2	2	2
D_c (g cm^{-3})	1.929	1.922	1.898
μ (mm^{-1})	2.231	2.222	17.675
data collected/unique	6485/2499	6348/2553	4088/1865
R_1 (>2σ/all data)	0.0683/0.0715	0.0617/0.0708	0.0787/0.0895
wR_2 (>2σ/all data)	0.1611/0.1626	0.1546/0.1581	0.2235/0.2294
GOF	1.053	1.010	1.024
residues (e Å^{-3})	−1.435/1.578	−1.299/0.818	−0.698/1.383

susceptibility measurements have been performed at frequencies of between 0.1 and 1500 Hz with an ac field of 0.0005 T and with a zero dc applied field. A powder sample of **1** was embedded in wax to avoid any field induced crystal reorientation. A diamagnetic correction of -1.8×10^{-4} cm^3/mol has been calculated from Pascal constants for **1** and embedding wax and has been applied to the observed magnetic susceptibility.

The Mössbauer spectral absorber contained 18 mg/cm^2 of a finely powdered sample of **1** dispersed in boron nitride, and the spectra have been obtained between 4.2 to 310 K on a constant acceleration spectrometer that utilized a rhodium matrix cobalt-57 source and was calibrated at room temperature with α-iron powder. Unless indicated explicitly, the relative error limits for the isomer shift, quadrupole splitting, line width, and percent area are ±0.005, ±0.01, and ±0.01 mm/s, and 0.2%. The absolute errors are approximately twice as large.

Synthetic Procedure. A mixture of 0.112 g or 2 mmol of iron powder and 0.648 g or 4 mmol of 1,4-chdcH$_2$, dissolved in 5 mL of H_2O, was sealed in a 23 mL Teflon-lined autoclave and heated at 220 °C for 3 days to give black needle-like crystals of **1**; the yield was 27% based on iron. The product was washed several times in an ultrasonic bath with deionized water and 95% ethanol to remove any excess 1,4-chdcH$_2$. The dried sample of **1**, used for elemental analyses, magnetic studies, and the infrared and Mössbauer spectral measurements, has been shown to be single phase by powder X-ray diffraction, see Supporting Information, Figure S1. IR data (ν, cm^{-1}): 3430(w), 2935(m), 2852(m), 1535(s), 1414(s), 1358(m), 1328(m), 1283(s), 1214(m), 1045(w), 974(w), 925(w), 776(m), 706(w), 612(w), 507(m), 487(m), and 436(w). Anal. Calcd for $Fe_2C_{12}H_{15}O_7$, **1**: C, 37.64; H, 3.95; Found: C, 37.80; H, 4.08%.

X-ray Crystallography. Single crystal X-ray diffraction data for **1** at 90 and 293 K have been obtained on a Bruker SMART Apex CCD diffractometer with Mo K$_\alpha$, $\lambda = 0.71073$ Å, radiation. The data for **1** at 473 K has been obtained on an Oxford Gemini S Ultra diffractometer with Cu K$_\alpha$, $\lambda = 1.54178$ Å, radiation. The structure has been solved with direct methods and refined with a full-matrix least-squares technique with the SHELXTL programs.[11] Data collection and structural refinement parameters are given in Table 1. The atom numbering scheme is shown in Supporting Information, Figure S2 and, in part, in Figure 1a. The CIF files for the structures of **1** obtained at 90, 293, and 473 K are provided in the Supporting Information.

Results and Discussion

[Fe^{II}Fe^{III}(μ_4-O)(1,4-chdc)$_{1.5}$]$_\infty$, **1**, where 1,4-chdc is the *trans*-1,4-cyclohexanedicarboxylate dianionic ligand, is air stable. Bond valence sum calculations[12] with $r_0(\text{Fe}^{II}-\text{O}) = 1.734$ Å and $r_0(\text{Fe}^{III}-\text{O}) = 1.759$ Å and the structural results presented below at 90 K yield an iron(II)-like valence of 2.15(1) for Fe1 and an iron(III)-like valence of 2.97(2) for Fe2, values that confirm the mixed-valent nature of **1** at lower temperatures. This mixed valence nature is fully supported by the Mössbauer spectral results obtained between 4.2 and 225 K, see below.

X-ray Structural Results. Single-crystal X-ray diffraction studies of **1** at 90, 293, and 473 K reveal no change in the triclinic $P\bar{1}$ space group or the crystallographic structure between 90 and 473 K. As is shown in Table 1 and Supporting Information, Figure S3, the *a*, *b*, and *c*-lattice parameters increase by 0.38, 0.67, and 1.39%, respectively, between 90 and 473 K; the corresponding changes in the α, β, and γ angles are relatively small. Thus, the increase of 10.9 Å^3 or 1.64% in the unit-cell volume of **1** between 90 and 473 K results predominately from an increase in the *c*-lattice parameter.

Because of the change in the iron valence states observed above about 225 K, see below, it is useful to investigate any changes in the iron positional parameters between 90 and 473 K. These changes, which are shown in Supporting Information, Figure S4, are small and are predominately centered on shifts of Fe1 and Fe2 along the *b*-axis with a smaller shift of Fe1 along the *c*-axis; other than these small shifts there is little change in the positional parameters between 90 and 473 K.

The X-ray structural results reveal that **1** contains two crystallographically distinct, pseudooctahedrally coordinated, Fe1 and Fe2 ions in [Fe1$^{II}_2$(μ_4-O)Fe2$^{III}_2$(μ_4-O)]$^{6+}$ chains oriented along the *a*-axis with the alternative, orthogonally arranged, Fe1^{II} and Fe2^{III} ions interconnected by μ_4-O dianions, dianions which have a pseudotetrahedral coordination environment, see Figure 1a,b. These chains are interconnected by the 1,4-chdc ligands in six-directions to form a three-dimensional iron-organic framework with a shortest interchain Fe···Fe distance of 9.40 Å at 293 K, see Figure 1c.

In spite of the absence of any dramatic changes in the crystal structure of **1** between 90 and 473 K, there are changes in the [Fe1$^{II}_2$(μ_4-O)Fe2$^{III}_2$(μ_4-O)]$^{6+}$ chain bonding, see Figure 2. Although there are relatively small changes in the average Fe−O bond distances upon warming, the shorter average Fe2−O iron(III)−oxygen bond distances at 90 K become slightly longer than the average Fe1−O iron(II)−oxygen distances at 293 and 473 K. Simultaneously, a similar, significant, change in the Fe1···Fe1 and Fe2···Fe2 non-bonded distances is observed; in contrast the μ_4-O to μ_4-O, O7···O7, non-bonded distance remains almost unchanged. These unexpected changes with temperature are, no doubt, associated with the partial electron delocalization that is observed above about 225 K, see below.

---

[11] (a) Sheldrick, G. M. *SADABS 2.05*; University of Göttingen: Göttingen, Germany, 2002. (b) *SHELXTL 6.10*; Bruker Analytical Instrumentation: Madison, WI, 2000.

[12] Brown, I. D.; Altermatt, D. *Acta Cryst., Sect. B* **1985**, *41*, 244.

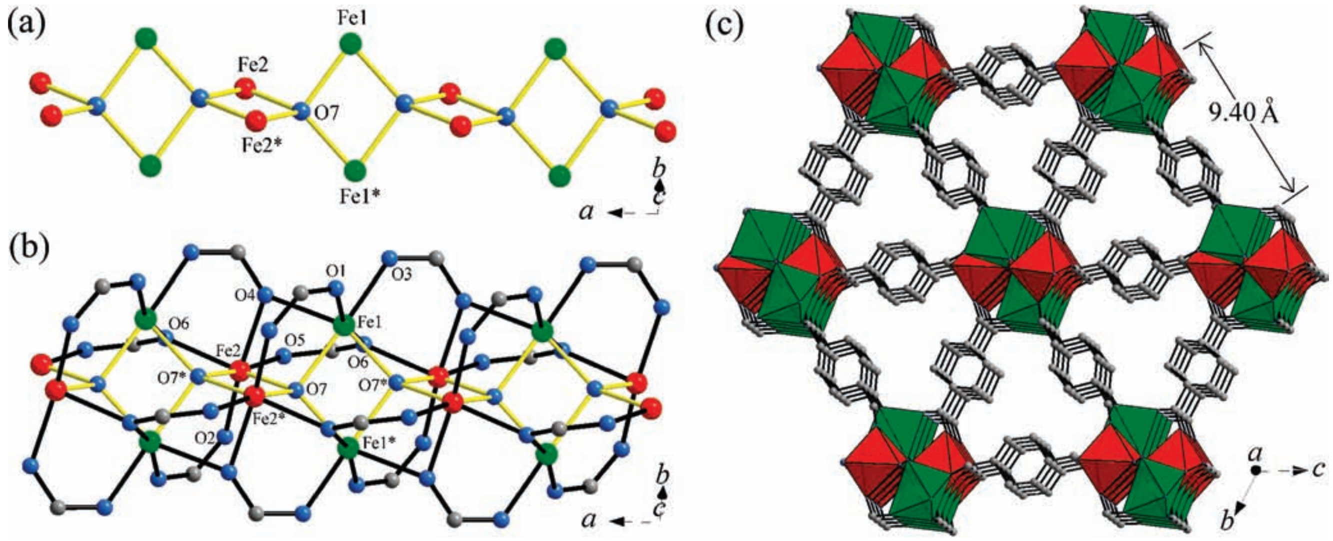

Figure 1. Carboxylate-supported tetrahedral chain, a and b, and the three-dimensional framework, c, viewed down the *a*-axis of **1**. The iron(II) Fe1 is green, the iron(III) Fe2 is red, the oxygen is blue, and the carbon is gray.

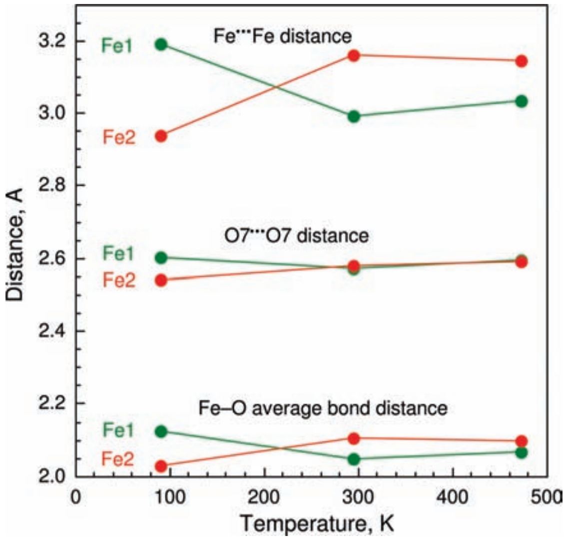

Figure 2. Temperature dependence of some of the distances found in the $[Fe1^{II}_2(\mu_4\text{-}O)Fe2^{III}_2(\mu_4\text{-}O)]^{6+}$ moiety that makes up the linear chains in **1**.

Magnetic Properties. The dc magnetic susceptibility of **1** has been measured from 2 to 320 K in an applied field of 0.010 T and the *M*/*H* ratio has been measured from 2 to 70 K in applied fields of 0.005 to 5 T, see Figure 3a and its inset.

At 300 K χT is 3.59(5) cm^3 K/mol, which corresponds to an effective magnetic moment, μ_{eff}, of 5.36(4) μ_B per mole of **1**. These values are substantially lower than the expected spin-only Curie constant of 7.38 cm^3 K/mol and effective magnetic moment of 7.68 μ_B per mole calculated for one high-spin iron(II) ion and one high-spin iron(III) ion. This difference may be explained by a combined influence of a significant antiferromagnetic coupling between the iron ions through the μ_4-O-bridge[13] and of the partial electronic delocalization along the chain observed above 225 K in the Mössbauer spectra, see below.

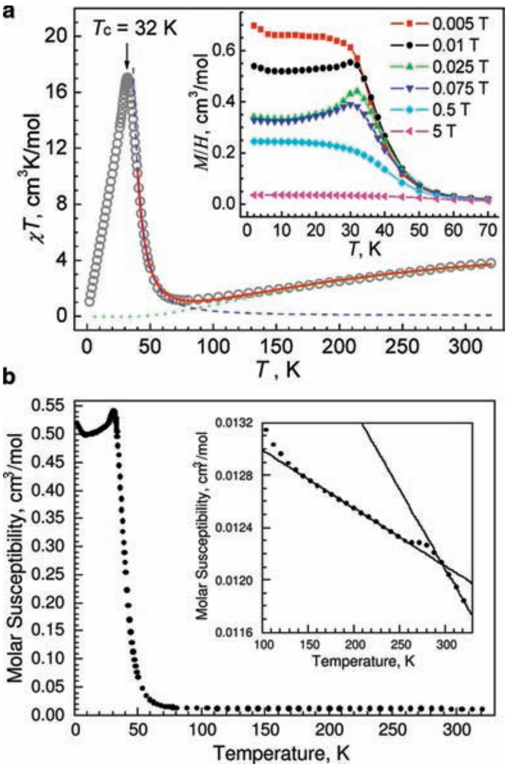

Figure 3. (a) Temperature dependence of χT of **1** obtained in a 0.01 T applied dc field. The red solid line corresponds to a fit of the high temperature behavior with eq 1, and the dotted green and the dashed blue lines correspond to the antiferromagnetic and ferromagnetic contributions found in eq 1. Inset: The temperature dependence of the molar *M*/*H* ratio of **1** obtained at the indicated applied dc fields. (b) The molar magnetic susceptibility of **1** obtained in a 0.01 T applied field. Inset: The expanded molar susceptibility of **1** obtained between 100 and 320 K showing the anomaly observed between 250 and 290 K.

Below 320 K χT decreases monotonically to reach a minimum of 1.14(2) cm^3 K/mol at 80 K and then increases up to a maximum of 17.0(4) cm^3 K/mol at 32 K, as is shown in Figure 3a. This high temperature behavior is expected for ferrimagnetic chains and/or compounds containing orbitally degenerate magnetic ions, such as iron(II) ions, whereas the large increase in χT below 80 K is expected for ferrimagnetic

---

[13] (a) Cannon, R. D.; White, R. P. *Prog. Inorg. Chem.* **1988**, *36*, 95. (b) Long, G. J.; Robinson, W. T.; Tappmeyer, W. P.; Bridges, D. L. *J. Chem. Soc., Dalton Trans.* **1973**, 573.

or spin-canted magnetic behavior resulting from the topology of the chain.

As will be discussed in the Mössbauer spectral results section below, **1** undergoes an electronic change between about 225 and 290 K, a change that is also reflected in its magnetic properties. Although this change is not apparent in Figure 3a, it is apparent in the molar susceptibility of **1** which is shown in Figure 3b; the anomaly becomes apparent in the expanded molar susceptibility of **1**, see the inset to Figure 3b. As shown in this inset, the slope of the temperature dependence of the molar susceptibility of **1** decreases from -4.40×10^{-6} cm^3/mol K between 150 and 250 K to -12.1×10^{-6} cm^3/mol K between 295 and 320 K.

The temperature dependence of *M/H* between 2 and 70 K measured in applied fields between 0.005 and 5 T is shown in the inset to Figure 3a. The steep increase in χT and *M/H* below 40 K is a clear indication that the chains carry a net magnetic moment in their ground state, a moment which saturates in large fields. Further, the field dependence of the magnetization measured between 7.5 and 12 K and shown in Figure 4a indicates the presence of weak ferromagnetism. At 12 K, the field dependence of the magnetization, its linear increase in fields above and below 1 T, and its rather small zero field extrapolated value of 0.22 μ_B are consistent with the presence of a canted or non-collinear magnetic structure for **1**. Upon cooling from 10 to 7.5 K, the field dependence of the magnetization exhibits hysteresis with coercive fields that increase from 0.028 to 2.772 T and remnant magnetization. Below 9 K the coercive field increases, but the hysteresis loops are not useful because the maximum 7 T field is insufficient to reach the reversible portion of the loop, as is observed at 7.5 up to 9 K. The lack of saturation also explains the decrease in the observed magnetization at high fields upon cooling from 12 to 8 K. Below 8 K, the ground-state coercive field for **1** is certainly much larger than 3 T. Such large coercive fields are not really surprising considering the low value of the net moment and the magnetic anisotropy of the iron(II) ions. By using the rather low 3.1 emu/cm^3 magnetization of **1** and an estimated coercive field at zero K of 5 T, a reasonable and rather small but reasonable magnetic anisotropy of 150 kOe/cm^3 or 0.7 K per iron(II) ion is obtained.

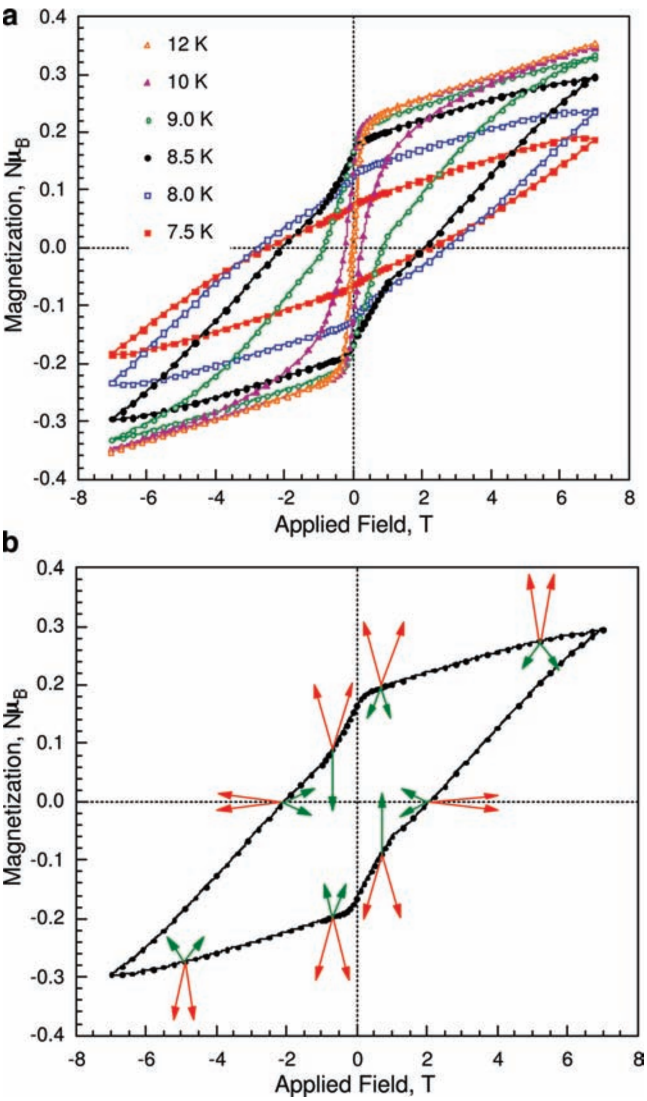

Figure 4. (a) Magnetic hysteresis observed in **1** at the indicated temperatures. (b) A diagrammatic sketch of the evolution of the "spin-fan" along the magnetization loop of **1** obtained at 8.5 K. The Fe1 iron(II) spin components are shown in green and the Fe2 iron(III) spin components are shown in red.

Upon consideration of the magnetic exchange pathways present within the $[\mathrm{Fe1^{II}}_2(\mu_4\text{-O})\mathrm{Fe2^{III}}_2(\mu_4\text{-O})]^{6+}$ chains of **1** and the low symmetry of the iron(II) site, the presence of spin canting, or a non-collinear magnetic structure, is not surprising. Indeed, because of the structure of the $[\mathrm{Fe^{II}}_2(\mu_4\text{-O})\mathrm{Fe^{III}}_2(\mu_4\text{-O})]^{6+}$ moiety, several different frustrated spin configurations may be anticipated. The spins of the isotropic, $^6A_{1g}$, high-spin pseudooctahedral iron(III) ions may be viewed as classical spins and are expected to orient in a direction that minimizes the energy of the magnetic chain. In contrast, the spins of the high-spin, approximately $^5T_{2g}$, pseudooctahedral iron(II) ions typically will minimize their energy by orienting within the pseudooctahedral equatorial plane, an anisotropic magnetic behavior that is known[14] as "easy-plane anisotropy." A spin Hamiltonian based theoretical description of the low-lying spin state of **1** is not straightforward because the sign and strength of the exchange interactions present are difficult to estimate. Therefore, to understand the low temperature magnetization loops and to propose a possible scheme for the low temperature spin configuration, the complex exchange interactions that take place in the edge sharing tetrahedral chain structure of **1** have been examined more closely without any a priori assumptions.

In a tetrahedrally arranged group of metal ions there are six composite exchange pathways between the metal ions, see Scheme 1. All these pathways include both, a direct pathway and multiple through-bond exchange pathways. The lengths observed at 90 K of the direct pathways are given at

---

[14] (a) Kajiwara, T.; Nakano, M.; Kaneko, Y.; Takaishi, S.; Ito, T.; Yamashita, M.; Igashira-Kamiyama, A.; Nojiri, H.; Ono, Y.; Kojima, N. *J. Am. Chem. Soc.* **2005**, *127*, 10150. (b) Oshio, H.; Hoshino, N.; Ito, T.; Nakano, M. *J. Am. Chem. Soc.* **2004**, *126*, 8805. (c) Oshio, H.; Nakano, M. *Chem.—Eur. J.* **2005**, *11*, 5178.

Scheme 1. Schematic Representation of the Four Combinations of Exchange Interactions That Lead to a Collinear Spin Configuration, A to D, for the Four Tetrahedrally Arranged Iron Ions in the $[Fe1^{II}_2(\mu_4\text{-}O)Fe2^{III}_2(\mu_4\text{-}O)]^{6+}$ Chains of **1**[a]

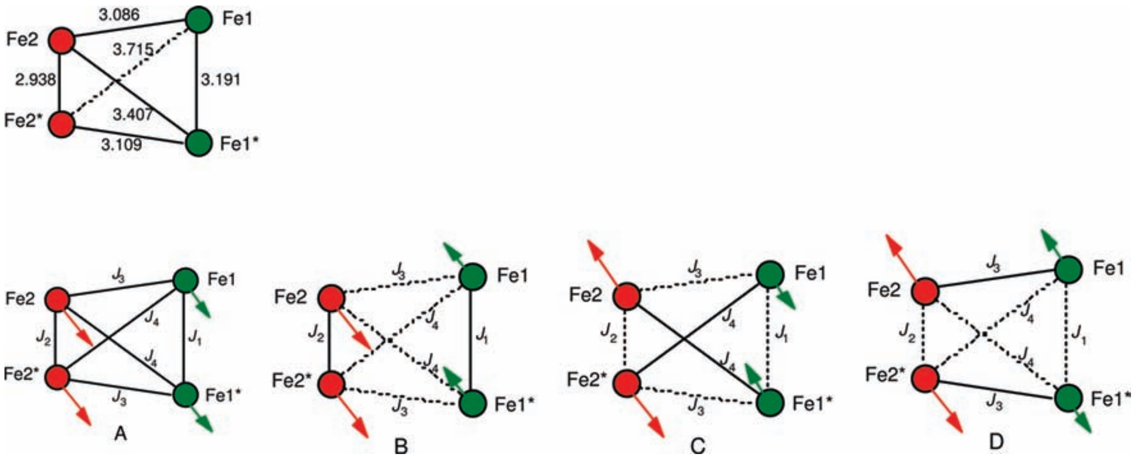

[a] The 90 K direct separation distances are given in ångström at the top of the figure. All other combinations lead to frustration on at least two of the triangular faces. For A to D the ferromagnetic exchange pathways, with $J_i > 0$, are given as solid lines and the antiferromagnetic exchange pathways, with $J_i < 0$, are given as dashed lines.

the top of Scheme 1, and the lengths of the Fe$-\mu_4$-O$-$Fe through bond pathways are given below. It should be noted that in addition to the Fe$-\mu_4$-O$-$Fe through bond pathways within one tetrahedron enumerated below there are additional Fe$-\mu_4$-O$-$Fe through bond pathways outside the tetrahedron. Further, there are additional Fe$-$O$-$C$-$O$-$Fe carboxylate bridged pathways that are not considered herein.

For the Fe1$-$Fe1* iron(II)$-$iron(II) pathway, referred to as J_1, there is one through-bond exchange pathway, Fe1$-\mu_4$-O7$-$Fe1*, with a pathway distance of 2.056 + 2.063 = 4.119 Å and a bond angle of 101.7°. For the Fe2$-$Fe2* iron(III)$-$iron(III) pathway, J_2, there is one through-bond exchange pathway, Fe2$-\mu_4$-O7$-$Fe2*, with a pathway distance of 1.902 + 1.982 = 3.884 Å and a bond angle of 98.3°.

For Fe1$-$Fe2 and Fe1*$-$Fe2* iron(II)$-$iron(III), J_3 and J_3', there are two slightly different direct pathways and one through-bond exchange pathway, Fe1$-\mu_4$-O7$-$Fe2, with a pathway distance of 2.056 + 1.982 = 4.038 Å and a bond angle of 99.7° and one through-bond exchange pathway, Fe1*$-\mu_4$-O7$-$Fe2*, with a pathway distance of 2.063 + 1.902 = 3.965 Å and a bond angle of 103.2°.

Finally, for Fe1$-$Fe2* and Fe1*$-$Fe2 iron(II)$-$iron(III), J_4 and J_4', there are two somewhat different direct pathways and there is one through-bond exchange pathway, Fe1$-\mu_4$-O7$-$Fe2*, with a pathway distance of 2.056 + 1.902 = 3.958 Å and one bond angle of 139.6° and a through-bond exchange pathway, Fe1*$-\mu_4$-O7$-$Fe2, with a pathway distance of 2.063 + 1.982 = 4.045 Å and a bond angle of 114.7°.

Therefore 64 different exchange schemes can be devised according to the sign of the J_i values, among which only four are unfrustrated. All other possible exchange schemes have at least two triangular faces with an odd number of antiferromagnetically coupled magnetic spins. The unfrustrated exchange schemes, see Scheme 1, are A with J_1 to $J_4 > 0$ corresponding to a ferromagnetic configuration, B with J_1 and $J_2 > 0$ and J_3 and $J_4 < 0$ corresponding to a ferrimagnetic configuration, and C and D, two schemes with J_1 and $J_2 < 0$ and J_3 and J_4 with opposite signs corresponding to two different antiferromagnetic configurations.

Among the four collinear configurations shown in Scheme 1, the only plausible candidate for **1** is B the ferrimagnetic configuration and the net spin only moment would be 2 μ_B per mole of **1.** However, the *g*-factor of iron(II) may be slightly larger than two and the iron(II) moment may approach that of iron(III) yielding the low observed net moment. However, this explanation has to be revised in view of some of the specific details observed in the magnetization loops of **1**. At 10 K and above, the *M*(*H*) loops, see Figure 4a, show a rapid saturation in a field of less than 0.5 T with no hysteresis; in larger fields, *M*(*H*) increases linearly. Thus above 10 K, the high field linear increase cannot result from magnetic anisotropy because of the absence of any hysteresis. Furthermore, the increase is perfectly linear whereas the presence of magnetic anisotropy would lead to a significant curvature for a powdered sample. The linear increase cannot result from the presence of some paramagnetic phase because it is accompanied by the occurrence of a net moment and its slope is temperature independent between 10 and 20 K. Finally, the rather large 0.018 Nμ_B/T slope of this linear increase is incompatible with Pauli paramagnetism. Therefore, this behavior of the magnetization is a clear indication of a non-collinearity in the spins and the existence of canted spins forming a "spin-fan" as is shown in Figure 4b, "spin-fans" that progressively close with increasing field. Spin canting may be a result of the Dzyaloshinskii$-$Moriya interaction, an interaction that is permitted by the structure of **1.** Indeed, whereas the Fe1 pairs and Fe2 pairs in the $[Fe1^{II}_2(\mu_4\text{-}O)Fe2^{III}_2(\mu_4\text{-}O)]^{6+}$ chains are related by centrosymmetry, the Fe1$-$Fe2 pairs are not. However, the existence of Dzyaloshinskii$-$Moriya interaction is not a necessary condition for the appearance of spin-canting because competing exchange interactions can lead to the same result. Therefore the existence of some frustration must be considered. Starting from the unfrustrated schemes this may be the

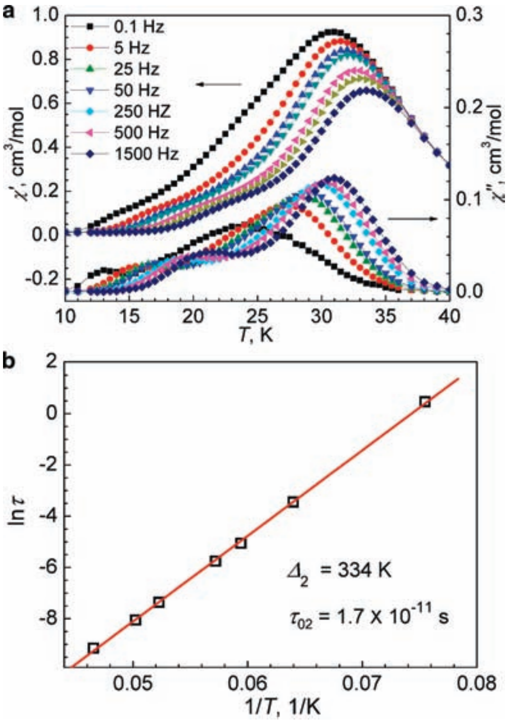

Figure 5. (a) Temperature dependence of the real and imaginary parts of the molar ac magnetic susceptibility of **1**, obtained at the indicated frequencies in a zero dc applied field. (b) The Arrhenius plot obtained for the minor maximum in χ'' of the molar ac magnetic susceptibility of **1**.

case whenever only one of the J_i values has an opposite sign to the one quoted in cases A to D of Scheme 1, which leads, at least, to two frustrated triangular faces.

A slight canting about the ferromagnetic A configuration cannot yield the small net moment that is observed and may be eliminated. A slight canting about the antiferromagnetic configurations of C or D is a plausible candidate as far as the small net moment and its linear increase with applied field are concerned. However, for such a perturbed antiferromagnetic structure the weak net moment is perpendicular to the main easy anisotropy axis. Therefore, it is unlikely that such a spin configuration could give rise to a large coercive field because its net moment can easily rotate as the field increases or decreases. Hence, a canting modification to the ferrimagnetic configuration, B, with a partially opened spin-fan between the iron(II) spins and the iron(III) spins, is proposed for **1**.

To gain further understanding in the spin structure in the chains, either ab initio calculations or spin dimer analysis, on the theoretical side, or magnetic neutron diffraction studies to be undertaken in the near future, may prove useful in unraveling the actual magnetic spin structure of **1**.

The presence of slow relaxation is also evident in the frequency-dependence of the in-phase, χ', and out-of-phase, χ'', magnetic susceptibility of **1** determined in an ac field of 0.0005 T, see Figure 5a. Both χ' and χ'' exhibit frequency dependent maxima. With increasing frequency, the main peak of χ' shifts very little from 31 to 33 K. On the low temperature side of the peak a poorly resolved shoulder can also be observed, a shoulder that shifts from 13 to 22 K with increasing frequency. In contrast, the main peak in χ'' shifts from 24 K at 0.1 Hz to 31 K at 1500 Hz, while a weaker maximum shifts from 13 to 21 or 22 K with increasing frequency in a fashion parallel to that of the shoulder observed for χ'. These maxima may correspond to the onset of three-dimensional magnetic ordering, spin freezing,[15] or single-chain magnetic[16] behavior.

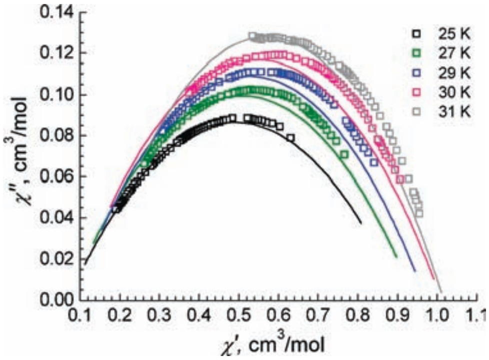

Figure 6. Cole−Cole χ'' vs χ' plot of the ac susceptibility of **1**. The solid lines correspond to fits with the generalized Debye model; the corresponding fit equations and parameters are given in Supporting Information, Table S1.

To clarify the origin of these peaks, an analysis of the dynamic response of the ac susceptibility, based on the Arrhenius $\tau = \tau_0 \exp(\Delta/T)$ law, has been undertaken. For the more intense peak in χ'' observed between 24 and 31 K, this analysis yields a non-physical value of the relaxation time, that is, $\tau_{01} = 5.9 \times 10^{-18}$ s, see Supporting Information, Figure S5. In contrast, the Arrhenius law analysis between 13.0 and 21.5 K, see Figure 5b, obtained by using the minor peak in χ'', yields $\Delta_2 = 334$ K and $\tau_{02} = 1.7 \times 10^{-11}$ s, values that are compatible with freezing,[15] single chain magnetic dynamics,[16] or superparamagnetic-like blocking. This energy barrier seems rather high for a single chain magnetic barrier but, as will be shown below, it is consistent with the exponential temperature dependence of the susceptibility observed above 32 K. This behavior suggests either the coexistence of short and long-range order in **1** or the reminiscence of **1** for its single chain magnetic dynamics even in its ordered state, vide infra. In the 25 to 31 K temperature range over which the main maxima of χ'' and χ' can be observed a Cole−Cole analysis has been performed, which shows a poor fit with the generalized Debye model and large α values between 0.645 and 0.742 indicate a broad distribution of relaxation time, see Figure 6 and Supporting Information, Table S1. These poor fits indicate that the dynamics of **1** is probably not governed by a single process near 30 K.[15] Unfortunately, no such Cole−Cole analysis could be performed over the 15 to 22 K temperature range of the secondary maximum in χ'' because of the large interference from the tail of the major peak. The most likely origin of the major peak in χ' and χ'' is the presence of critical fluctuations close to an ordering transition at 32 K as suggested by the weak frequency dependence of the peak of χ'. Above this temperature and over the limited interval 0.028 and 0.015 K^{-1}, or 36 and 66 K, both $\ln(\chi_{dc}T)$ versus

---

(15) Mydosh, J. A. *Spin Glasses: An Experimental Introduction*; Taylor & Francis: London, 1993.

(16) Coulon, C.; Miyasaka, H.; Clérac, R. *Struct. Bonding (Berlin)* **2006**, *122*, 163.

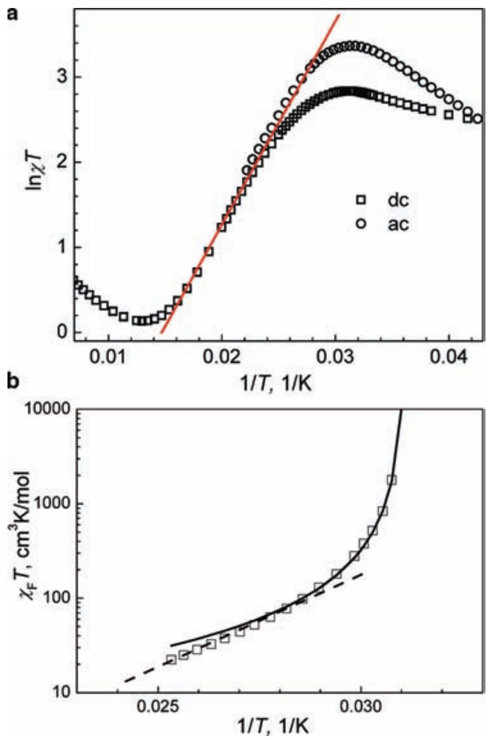

Figure 7. (a) Logarithm of the observed $\chi_{ac}T$ and $\chi_{dc}T$ as a function of the inverse temperature showing an exponential one-dimensional regime between 40 and 60 K. Deviations at high and low temperature are due to the dominant antiferromagnetic exchange coupling between ions at high temperatures and three-dimensional ordering at low temperatures. (b) The semilogarithmic plot of $\chi_F T$ as a function of the inverse temperature. Single chain magnetic behavior corresponds to the dashed line, and the three-dimensional ordering magnetic behavior corresponds to the solid line.

$1/T$ and $\ln(\chi'_{ac}T)$ versus $1/T$ clearly show an exponential variation in the correlation length that is in agreement with single chain magnetic behavior, see Figure 7a. It should be noted that this behavior is identical to that described by the dashed blue curve in Figure 3a. The following "non-critical scaling" analysis[17,18] suggests that, after the development of spin correlation in the chains, **1** undergoes a three-dimensional magnetic ordering below 32.16 K.

Scaling Theory Analysis. Both the magnitude of the spontaneous magnetization and the high-field dependence of the magnetization support the existence of a non-collinear low-lying spin configuration within the $[\mathrm{Fe^{II}}_2(\mu_4\text{-O})\mathrm{Fe^{III}}_2(\mu_4\text{-O})]^{6+}$ chain. The combined influence of ferrimagnetism,[19] canting, and spin-orbit coupling in **1** results in a well-defined minimum in the temperature dependence of χT, in the paramagnetic regime above 80 K in **1**, see Figure 3a. A recently developed "non-critical scaling" theory[17,18] has shown that this minimum is well described by the sum of two exponential functions,

$$\chi T = C_1 \exp(E_1/T) + C_2 \exp(E_2/T) \qquad (1)$$

where $C_1 + C_2$ is the high temperature extrapolated Curie constant per mole of compound or, in the case of **1**, per formula of **1**. The first term in eq 1 represents a ferromagnetic contribution that is dominant at low temperatures, whereas the second term represents a high-temperature antiferromagnetic contribution that vanishes at 0 K. The fit with eq 1 of the magnetic susceptibility of **1** between 50 and 320 K, a temperature range over which the influence of the suspected ordering transition at 32 K is negligible, is shown as the red curve in Figure 3a and yields $C_1 = 0.020(3)$ cm^3 K/mol, $E_1 = 254.3(1)$ K, $C_2 = 6.710(1)$ cm^3 K/mol, and $E_2 = -195.4(4)$ K, for the ferromagnetic and antiferromagnetic contributions, contributions that are shown in Figure 3a as the blue dashed and green dotted curves, respectively. The four parameters used in the first step of the present analysis have a fundamental physical meaning. As expected, at room temperature the extrapolated Curie constant, $C_1 + C_2 = 6.73$ cm^3 K/mol, is in much better agreement with the expected value of 7.375 cm^3 K/mol than the observed value of 3.593 cm^3 K/mol. The interactions that are responsible for the initial decrease in χT between 320 and 80 K result from the dominant intrachain interactions. In contrast, below about 70 K χT is dominated by the first, ferromagnetic, term in eq 1, a term that corresponds to the increase in the intrachain ferromagnetic correlation length as described in the Glauber model,[20] with, however, reduced effective spins in the one-dimensional chain. Further, the energy E_1 obtained for the non-critical increase in susceptibility is similar to the value of the barrier, 334 K, obtained above for the relaxation at low temperature, a similarity which suggests the persistence of Glauber dynamics below 30 K. To investigate in detail the low-temperature behavior, the antiferromagnetic contribution, dominant above 80 K, has been subtracted from χT and the resulting $\chi_F T = \chi T - C_2 \exp(E_2/T)$ is discussed in the next paragraph below 50 K, the temperatures at which it represents the main contribution to the total susceptibility.

As discussed above, the peaks in χ_{ac} and χT at about 32 K cannot be explained by a simple exponential increase of the relaxation time and of the correlation length in a single-chain magnet. Therefore the possibility of three-dimensional ordering must be considered. In the thermodynamic limit the dc susceptibility is expected to diverge at the Curie temperature when long-range ordering occurs. However, in actual experiments, the observed susceptibility saturates at some finite value χ_s below T_c, see inset of Figure 3a, because of the non-zero demagnetizing field, a non-zero applied field, finite time, and finite grain size effects. Therefore, to analyze the critical behavior, the observed magnetic susceptibility has been corrected as follows by

$$\chi_F T = T/(\chi^{-1} - \chi_s^{-1}) \qquad (2)$$

where $\chi_s^{-1} = 1.89$ mol/cm^3, obtained from the maximum in *M/H* at 0.01 T, see inset in Figure 3a, accounts for the saturation of χ due to the demagnetizing field and other extrinsic effects. The corrected susceptibility, χ_F, may now be investigated within the framework of Souletie's model[17,18] for critical phenomena in which χT is given by

---

[17] (a) Souletie, J.; Rabu, P.; Drillon, M. *Phys. Rev. B* **2005**, *72*, 214427. (b) Souletie, J.; Rabu, P.; Drillon, M. In *Magnetism: Molecules to Materials, V*; Miller, J. S.; Drillon, M., Eds.; Wiley-VCH: Weinheim, 2005; pp 347−377.

[18] Drillon, M.; Panissod, P.; Rabu, P.; Souletie, J.; Ksenofontov, V.; Gütlich, P. *Phys. Rev. B* **2002**, *65*, 104404.

[19] Curely, J.; Georges, R.; Drillon, M. *Phys. Rev. B* **1986**, *33*, 6243.

[20] Glauber, R. J. *J. Math. Phys.* **1963**, *4*, 294.

$$\chi T = C_{\mathrm{eff}}(1 - T_c/T)^{-\gamma} \qquad (3)$$

where χ herein is given as χ_F. Unlike the classical approach, eq 3 is not restricted to a narrow critical regime, that is, a regime very close to T_c; in the high temperature limit eq 3 yields the Curie−Weiss law.

In a second step of the analysis, a semilog plot of $\chi_F T$ versus $1/T$ reveals a clear change over from an exponential behavior above 36 K, that is, below 0.028 K^{-1}, see the straight dashed line in Figure 7b, a behavior that is characteristic of the single-chain dynamics, to a power law behavior, $\chi_F T = 2.95(1 - 32.16/T)^{-1.40}$, below 36 K, a power law that indicates the occurrence of long-range spin−spin correlations.[17] Again it should be noted that this behavior is identical to that described by the dashed blue curve in Figure 3a. Then $C_{\mathrm{eff}} = S(S + 1)/2 = 2.95$ provides an estimate of the net "effective" spin of the chain, namely "$S \sim 2$," as a result of the combined effect of the superexchange interactions between neighboring ions and the presence of anisotropy for the iron(II) ions. The critical exponent $\gamma = 1.40$ obtained from the fit is consistent with three-dimensional ferromagnetic ordering. However, because of the various steps in the mathematical treatment and corrections applied to obtain $\chi_F T$, the existence of long-range order is suggested but not confirmed. This long-range magnetic ordering would take place at $T_c = 32.16$ K, most likely through the coupling of the magnetic chains by the 1,4-chdc bridging ligands with a possible additional dipolar coupling between chains.[21,22]

As indicated above, the transition of **1** toward three-dimensional order does not lead to fully blocked spins because residual time fluctuations are observed in χ' and χ'' below 32 K, fluctuations that slow as the temperature decreases and eventually freeze below 15 K. Therefore, three different magnetic behavior regimes are observed in **1** between 2 and 320 K. Above 36 K, **1** may be described as a one-dimensional ferrimagnetic-like compound.[21] Frustration alone can give rise to such behavior when the frustration originates from competing exchange interactions between iron(II) and iron(III) ions. Between 36 and 25 K, the interchain interactions are no longer negligible, as is indicated by the temperature dependence of χT and, as a result, the compound orders at 32.16 K. However, in this presumably ordered state, some residual fluctuations are still observed and the magnetization curves do not show any coercivity above 12 K. Below 25 K the residual fluctuations slow and eventually freeze below 15 K. The small net moment of 0.22 μ_B per mole of **1** may be attributed to a non-collinear or canted spin structure of the spins of the four iron ions in the $[\mathrm{Fe^{II}}_2(\mu_4\text{-O})\mathrm{Fe^{III}}_2(\mu_4\text{-O})]^{6+}$ chains. The slow relaxation dynamics of the spins below 32 K may result from hopping between two different canting orientations. However, it has been shown that single-chain dynamic magnetic behavior can still persist below the three-dimensional ordering temperature.[23] Therefore, the observed dynamic behavior could equally be reminiscent of single-chain magnetic behavior for **1** with an energy barrier, Δ_2, of 254−334 K. Indeed, except for the canted nature of the net moment, the low temperature magnetic behavior of **1** is quite similar to that of $[\mathrm{Co(hfac)_2NIT\text{-}C_6H_4O(CH_2)_3CH_3}]_n$ which has recently been studied by Ishida and co-workers.[24]

Mössbauer Spectral Results. The Mössbauer spectra of **1** have been measured between 4.2 and 310 K; the 85 to 310 K spectra are shown in Figure 8 and the 4.2 to 65 K spectra are shown in Figure 9. The 4.2 to 65 K spectra indicate that the magnetic ordering or slow relaxation in **1** first begins to occur upon cooling below about 50 K, is partly established at 40 K, and is fully developed at 32 K; both the iron(II) Fe1 and iron(III) Fe2 ions exhibit sharp magnetic sextets between 4.2 and 32 K. The 4.2 to 65 K spectra have been fit with a superposition of sextets and doublets. The solid lines in Figures 8 and 9 are the results of the fits, and the resulting spectral parameters are given in Table 2. The isomer shifts of the spectral components of about 0.57 and 1.26 mm/s permit their unambiguous assignment to the iron(III) Fe2 and iron(II) Fe1 ions with a 50:50 relative population. At 4.2, 22, and 32 K, the large hyperfine field of about 49 T observed for the iron(III) ions is typical[25] of high-spin iron(III) ions. In contrast, the hyperfine field of about 7 T observed for the iron(II) ions is small[25] in comparison with the about 44 T field expected for high-spin iron(II) ions. Such small fields have already been observed in mixed valence iron oxalates[25] and result from the subtraction of large orbital and dipolar contributions to the hyperfine field from the typical core contribution of 44 T.

The presence of sharp sextets in the Mössbauer spectra at and below 32 K does not *necessarily* imply the existence of long-range magnetic ordering of the iron moments. Indeed, similar sharp sextets have been observed[25] in the presence of magnetic correlations over a distance of about 50 Å. Hence, the Mössbauer spectra obtained at 4.2, 22, and 32 K are compatible with long- or short-range magnetic ordering of the iron spins, in agreement with the conclusion drawn above from the magnetic susceptibility measurements.

The sharp sextets observed in the 4.2 and 22 K Mössbauer spectra are indicative of either a static ground-state three-dimensional magnetic structure or a relaxation process with a relaxation time[26] longer than 5×10^{-9} s. This is consistent with the magnetic measurements, which indicate, from the Arrhenius fit shown in Figure 5b, that the relaxation time is longer than 1 μs at temperatures below 32 K. However, if the residual fluctuations arise from hopping between two canted structures, the Mössbauer spectra should show two sextets associated with the two structures. These sextets are expected to differ by only the dipolar field, a contribution to the hyperfine field that may be small. The observed line

---

(21) Drillon, M.; Panissod, P. *J. Magn. Magn. Mater.* **1998**, *188*, 93.

(22) Laget, V.; Hornick, C.; Rabu, P.; Drillon, M.; Turek, P.; Ziessel, R. *Adv. Mater.* **1998**, *10*, 1024.

(23) (a) Sessoli, R. *Angew. Chem., Int. Ed.* **2008**, *47*, 2. (b) Zumer, S. *Phys. Rev. B* **1980**, *21*, 1298.

(24) Ishii, N.; Okamura, Y.; Chiba, S.; Nogami, T.; Ishida, T. *J. Am. Chem. Soc.* **2008**, *130*, 24.

(25) Carling, S. G.; Hautot, D.; Watts, I. D.; Day, P.; Visser, D.; Ensling, J.; Gütlich, P.; Long, G. J.; Grandjean, F. *Phys. Rev. B* **2002**, *66*, 104407.

(26) Mørup, S.; Oxborrow, C. A.; Hendriksen, P. V.; Pedersen, M. S.; Hanson, M.; Johansson, C. *J. Magn. Magn. Mater.* **1995**, *140−144*, 409.

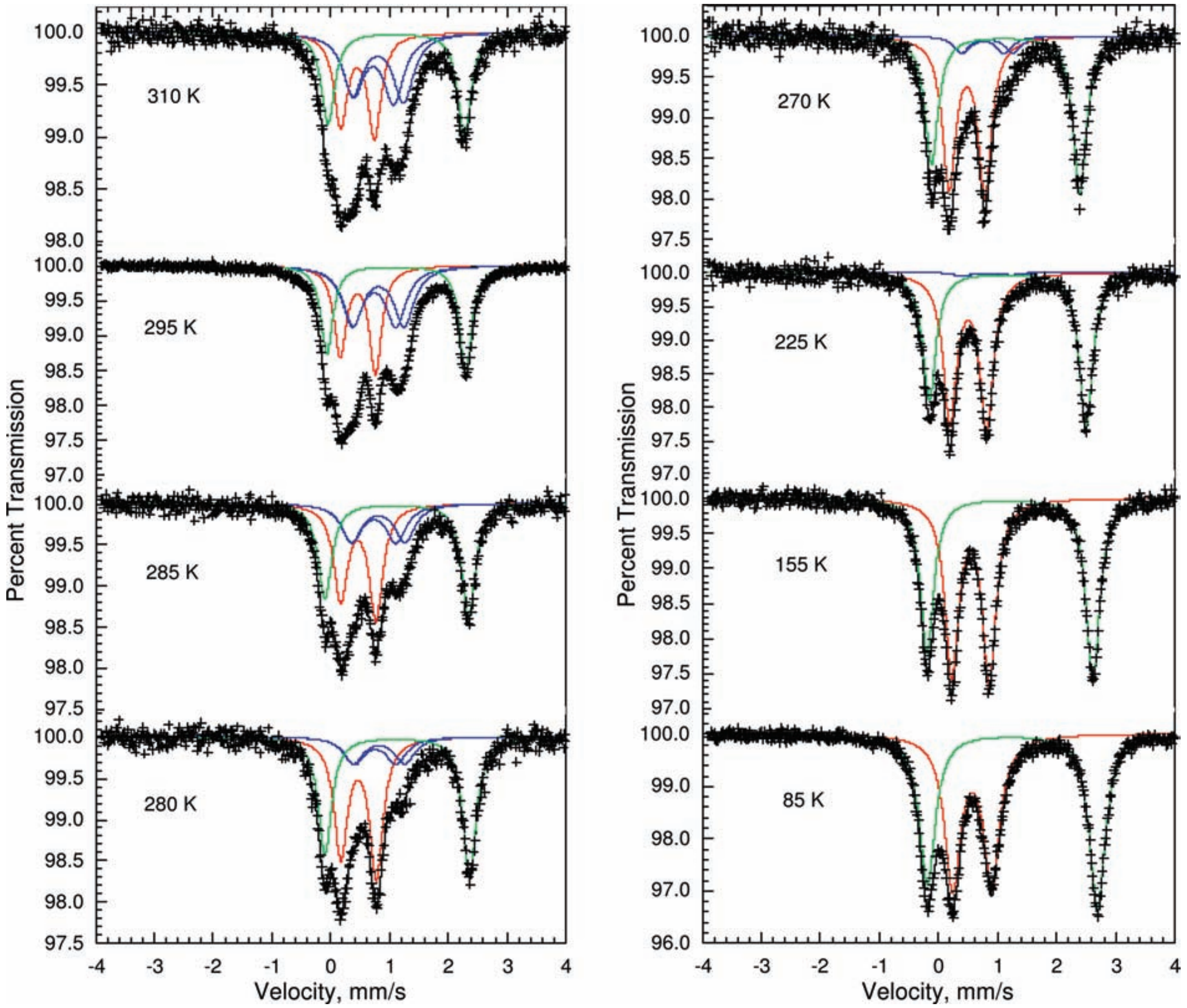

Figure 8. Paramagnetic iron-57 Mössbauer spectra of **1** obtained at the indicated temperatures. The green, red, and blue solid line components are assigned to iron(II) Fe1, iron(III) Fe2, and intermediate valent iron(II/III) ions, respectively.

width of about 0.3 mm/s at 4.2 and 22 K is only slightly larger than the calibration line width of the external lines of α-iron. Hence, if this slight broadening results from the presence of two sextets, their hyperfine fields do not differ by more than about 0.5 to 1 T. Hence, the Mössbauer spectra cannot distinguish between the two possible interpretations of the low-temperature magnetic measurements. Either a static magnetic ground state or a slow relaxation between two magnetic states will be indistinguishable at the resolution of the iron-57 Mössbauer spectra.

The small observed iron(II) field of 7 T may be a transferred field from the neighboring non-relaxing iron(III) ions. In this case the iron(II) spins are still fluctuating fast on the Mössbauer time scale in a zero applied field below 32 K. In the applied field of the magnetic measurements, the iron(II) spins may undergo a metamagnetic transition below 15 K. However the magnetization steps associated with a metamagnetic transition are usually observed in the first and third quadrants of the magnetization loops, steps which are not observed in Figure 4. Thus, it seems that the iron(II) spins are frozen at these low temperatures.

The observation of magnetic sextets with a large hyperfine field above 32 K and more specifically at 40 K indicates that short-range magnetic ordering or slow relaxation of the iron(III) spins occurs between 65 and 40 K in agreement with the observed increase in χT over this temperature range, see Figure 3a, and the change from an exponential to a power-law magnetic regime in Figure 7b.

The Mössbauer spectra of **1** between 85 and 310 K are shown in Figure 8, and the resulting fit parameters are given in Supporting Information, Table S2. At 85 and 155 K, the spectra have been fit with two quadrupole doublets, shown in green and red, with relative areas close to 50:50, doublets that, on the basis of their isomer shifts, are assigned to the iron(II) Fe1 and iron(III) Fe2 ions, respectively. The spectra at 300 and 310 K have been fit with four quadrupole doublets with relative areas constrained to 25:25:25:25. Two of these doublets, shown in green and red, have isomer shifts that are typical of iron(II) Fe1 and iron(III) Fe2 ions and the other two, shown in blue, have isomer shifts that are intermediate between and close to the average of the iron(II) and iron(III) ions. The quadrupole doublets shown in blue indicate the occurrence of electron delocalization in **1**. The spectra between 225 and 310 K have been fit with four doublets whose relative areas were varied. The use of two doublets assigned to the intermediate valence iron(II/III) ions is

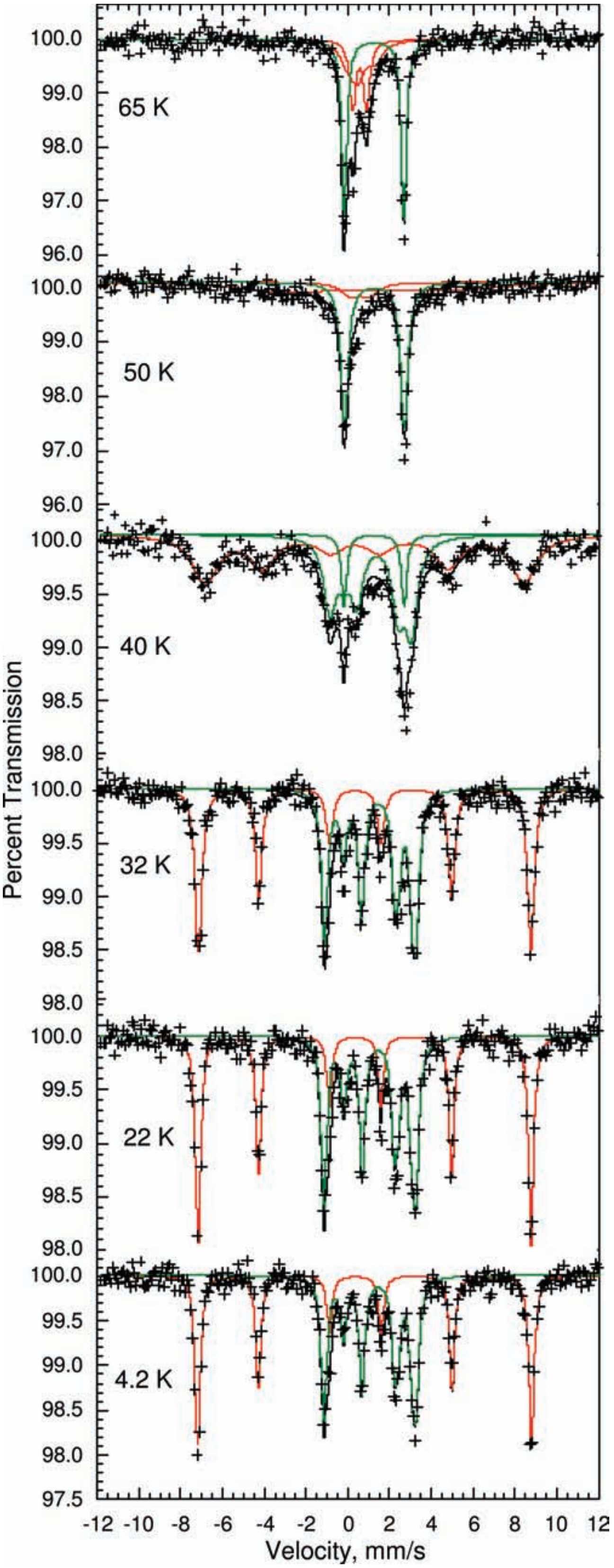

Figure 9. Magnetically ordered iron-57 Mössbauer spectra of **1** obtained at the indicated temperatures. The green and red solid line components are assigned to iron(II) Fe1 and iron(III) Fe2 ions, respectively.

justified by the exceedingly large line width and poor fits observed if only one doublet is used to fit the contribution assigned to these intermediate valence ions. A physical explanation for the presence of the two intermediate valence doublets is given below.

The temperature dependence of the spectral parameters between 4.2 and 310 K is shown in Figures 10 and 11. The temperature dependence of the isomer shifts of the components assigned to iron(II) Fe1 and iron(III) Fe2 ions is well fit with the Debye model,[27] and the resulting Mössbauer temperatures of 304(11) and 272(37) K are obtained, respectively. The isomer shifts of the intermediate valence iron ions are close to the average isomer shift of the iron(II) and iron(III) ions, an average that is shown by the blue solid line in Figure 10. Hence, the intermediate valence observed on these ions is equal to or at least close to 2.5.

Because the sign of the quadrupole splitting cannot be obtained from the paramagnetic Mössbauer spectra alone, the temperature dependence of the quadrupole splitting must be studied between 4.2 and 310 K to determine both the sign and the magnitude of the quadrupole splittings at the iron(II), iron(III), and intermediate valence iron(II/III) ions. The characteristic iron(II) profile observed at 4.2, 22, and 32 K consists of a triplet at lower velocities and a doublet at higher velocities, a relative location that indicates[28] that the quadrupole splitting, ΔE_Q, is positive. Because the quadrupole splittings of the intermediate valence iron ions are expected to be close to the average of the iron(II) and iron(III) quadrupole splittings, the iron(III) quadrupole splitting must then be assumed to be negative. The temperature dependence of the quadrupole splittings shown in Figure 11 uses these signs.

The temperature dependence of the iron(II) Fe1 quadrupole splitting, see Figure 11, has been fit with the Ingalls[29] model with a zero temperature quadrupole splitting of 2.86 mm/s and a crystal field splitting of 403 cm^{-1}. To account for the observed positive quadrupole shift in the magnetic iron(III) sextets at 4.2, 22, and 32 K with a negative quadrupole splitting, an angle, θ, of 90° between the principal component of the electric field gradient and the hyperfine field was introduced into the fits, as is indicated in Table 2. The fitted quadrupole splitting of about -0.90 mm/s for iron(III) Fe2 is well defined at and below 40 K but much less so at 50 and 65 K, where it was constrained to this value. In the paramagnetic spectra, the absolute value of the iron(III) quadrupole splitting is smaller than 0.90 mm/s. Hence, there seems to be a discontinuity in the temperature dependence of the iron(III) quadrupole splitting between 65 and 85 K, a discontinuity that most likely is associated with a subtle structural change, that is, magnetostriction, associated with any magnetic ordering. The temperature dependence of the iron(III) quadrupole splitting is also discussed below in an alternative treatment of the electron delocalization observed in the Mössbauer spectra.

The temperature dependence of the relative areas of the iron(II) Fe1, iron(III) Fe2, and intermediate valence iron(II/

---

(27) Shenoy, G. K.; Wagner, F. E.; Kalvius, G. M. In *Mössbauer Isomer Shifts*; Shenoy, G. K., Wagner, F. E., Eds.; North Holland: Amsterdam, 1978; p 51.

(28) Grant, R. W. In *Mössbauer Effect Methodology*; Gruverman, I. J., Ed.; Plenum Press: New York, 1966; Vol. 2, p 23.

(29) Ingalls, R. *Phys. Rev.* **1964**, *133*, A787.

Table 2. Mössbauer Spectral Parameters[a] of Magnetically Ordered **1**[a]

T, K	H, T	δ, mm/s[b]	ΔE_Q, mm/s	Γ, mm/s	θ, deg	area, %	assignment
65	0.00	1.258(4)	2.85(1)	0.32(1)		50	Fe1, iron(II)
	0.00	0.57	−0.90	0.32(1)		22(8)	Fe2, iron(III)
	2.9(8)	0.57	−0.90	0.80(11)	90.0	28(8)	Fe2, iron(III)
50	0.00	1.272(5)	2.87(1)	0.42(2)		50	Fe1, iron(II)
	0.00	0.57	−0.90(1)	1.1(2)		11(1)	Fe2, iron(III)
	27(3)	0.57	−0.90(1)	4.4(9)	90.0	39(1)	Fe2, iron(III)
40	0.00	1.257(1)	2.88(2)	0.30(2)		8(1)	Fe1, iron(II)
	5.1(1)	1.257(1)	2.88(2)	0.70(3)	82.9	42(1)	Fe1, iron(II)
	47.2(2)	0.57(3)	−0.90(1)	1.43(7)	90.0	50	Fe2, iron(III)
32	7.07(5)	1.268(5)	2.87(1)	0.37(1)	82.43(1)	50.0(8)	Fe1, iron(II)
	49.22(4)	0.580(5)	−0.93(2)	0.39(1)	90.0(1)	50.0(8)	Fe2, iron(III)
22	7.34(4)	1.260(4)	2.84(1)	0.32(1)	82.07(1)	50.1(8)	Fe1, iron(II)
	49.31(2)	0.575(3)	−0.92(1)	0.29(1)	90.0(1)	49.9(8)	Fe2, iron(III)
4.2	7.27(4)	1.262(4)	2.86(1)	0.33(1)	82.54(1)	50.4(8)	Fe1, iron(II)
	49.47(3)	0.579(3)	−0.90(1)	0.30(1)	90.0(1)	49.6(8)	Fe2, iron(III)

[a] The statistical errors are given in parentheses. Parameters with no indicated error have been constrained to the value given. [b] The isomer shifts are given relative to room temperature α-iron powder.

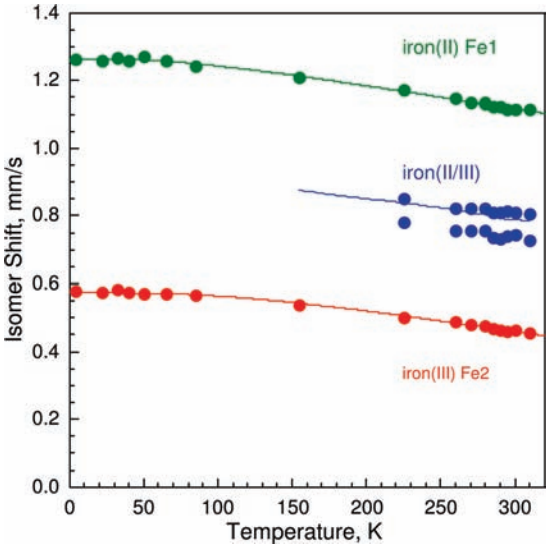

Figure 10. Temperature dependence of the isomer shifts in **1**. The green and red solid lines are the result of a fit with the Debye model. The blue line is the average of the iron(II) and iron(III) isomer shifts.

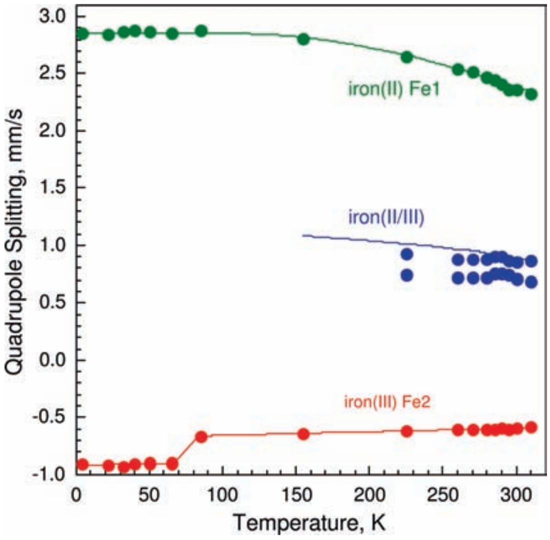

Figure 11. Temperature dependence of the quadrupole splittings in **1**. The green solid line is the result of a fit with the Ingalls model. The blue line is the average of the iron(II) and iron(III) quadrupole splittings. The red line is a guide to the eye.

III) ions is shown in Figure 12. Further, the temperature dependence of the logarithm of the total spectral absorption area is shown in Figure 13 and has been fit[27] with the Debye model; the resulting Debye temperature is 168(3) K. Figure 12 clearly indicates that the electron delocalization is activated above 225 K. In view of the 50% of intermediate valence iron ions and 25% each of iron(II) and iron(III) ions present at 295, 300, and 310 K, one is forced to conclude that at these temperatures only half the iron ions participate in the electron delocalization mechanism.

Rather surprisingly, the Mössbauer spectra obtained between 280 and 310 K, see Figure 8, do not show any broadening of the absorption lines and specifically of the iron(II) line at about 2.4 mm/s, as would be expected[30] and has been observed[31−33] many times, for a relaxation process in which the delocalized electron is thermally activated over a barrier separating two minima in the potential energy surface. Further the Mössbauer spectra of **1** obtained between 270 and 310 K reveal the simultaneous presence of iron(II), iron(III), and two iron(II/III) doublets with temperature dependent relative areas. Similar but not identical observations have been reported[34−36] earlier.

The same unusual absence of broadening of the Mössbauer spectral lines in the presence of valence detrapping or electron delocalization has been observed[34] in μ_3-oxo-bridged Fe_3O complexes and explained as follows. At low temperatures, one minimum in the potential energy surface is substantially lower than the other, and the electron is localized on the iron(II) ions. As the temperature increases,

---

(30) Grandjean, F. In *The Time Domain in Surface and Structural Dynamics*; Long, G. J., Grandjean, F., Eds.; Kluwer: Dordrecht, 1988; Vol. 228, p 287.

(31) Prietsch, M.; Wortmann, G.; Kaindl, G.; Schogl, R. *Phys. Rev. B* **1986**, *33*, 7451.

(32) Litterst, F. J.; Amthauer, G. *Phys. Chem. Miner.* **1984**, *10*, 1432.

(33) Angst, M.; Hermann, R. P.; Schweika, W.; Kim, J. W.; Khalifah, P.; Xiang, H. J.; Whangbo, M. H.; Kim, D. H.; Sales, B. C.; Mandrus, D. *Phys. Rev. Lett.* **2007**, *99*, 256402.

(34) Wu, C.-C.; Jang, H. G.; Rheingold, A. L.; Gütlich, P.; Hendrickson, D. N. *Inorg. Chem.* **1996**, *35*, 4137.

(35) Dong, T.-Y.; Hendrickson, D. N.; Iwai, K.; Cohn, M. J.; Geib, S. J.; Rheingold, A. L.; Sano, H.; Motoyama, I.; Nakashima, S. *J. Am. Chem. Soc.* **1985**, *107*, 7996.

(36) Dong, T.-Y.; Kambara, T; Hendrickson, D. N. *J. Am. Chem. Soc.* **1986**, *108*, 4423.

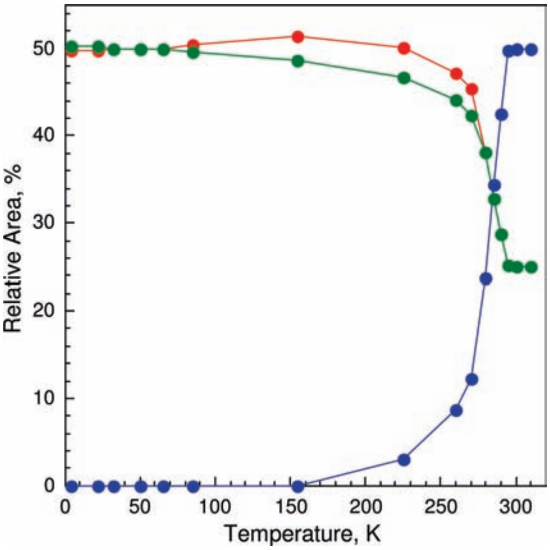

Figure 12. Temperature dependence of the relative areas of the Mössbauer spectral components of **1**. The iron(II), iron(III), and intermediate valent iron(II/III) ions are shown in green, red, and blue, respectively.

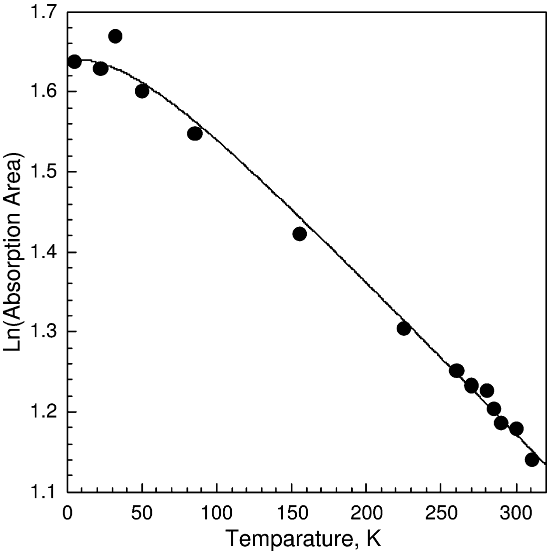

Figure 13. Temperature dependence of the logarithm of the total spectral absorption area. The solid line is the result of a fit with the Debye model.

the potential energy surface changes its shape because of small structural changes, and the two minima occur at the same energy. In this case, the electron can quantum mechanically tunnel between equal energy vibronic states at a rate faster than the Mössbauer time scale of 10^{-9} s; such temperature independent tunneling frequencies between vibronic states are expected to be of the order of 1 to 5 GHz.

The Mössbauer spectra of mixed-valence biferrocenium salts have been reported by Hendrickson and co-workers,[35,36] who have observed two types of Mössbauer spectra. In the first, the so-called "fusion-type" spectra, the well defined iron(II) and iron(III) doublets, associated with charge ordering or charge localization observed at low temperature, converge smoothly with increasing temperature with no line broadening toward a final average iron(II/III) doublet. In the second, the so-called "co-existence-type" spectra, the iron(II) and iron(III) doublets coexist with the average iron(II/III) doublet(s) over an extended temperature range, with relative areas that are temperature dependent.

The "fusion-type" Mössbauer spectra result from a progressive electron detrapping with increasing temperature, a detrapping that takes place through vibronic coupling, in a fashion similar to that invoked above, between the iron 3d orbitals and is fast at all temperatures on the Mössbauer time scale. The thermal evolution of the system is typical of a second-order order−disorder transition.[37] The "co-existence-type" spectra result from a relaxation through vibronic coupling between two thermally occupied orbitals on each iron ion. Hence, in this case the Mössbauer spectra consist of four doublet components,[38] two with no delocalization and two corresponding to the two possible delocalization pathways. The coexistence of the localized and delocalized components requires two different relaxation rates, a slow relaxation between states based on different orbitals and a fast relaxation between states based on the same orbital. In this two-orbital approach, the inclusion of a cooperative ligand field leads to a first-order charge order−disorder transition, a transition that is accompanied by a substantial entropy change. A cooperative two-orbital vibronic model of mixed-valence salts predicts[39] a wide variety of transitions from the low temperature ordered phase to the high-temperature disordered phase, that is, second-order and first-order transitions, re-entrant phase transitions, and two-step transitions.

In contrast to the present work, all of the above experimental and theoretical studies deal with low-spin iron(II) and iron(III) ions, ions in which the d_{xy} and the $d_{x^2-y^2}$ orbitals are involved in the charge relaxation process. In the theoretical studies, the isomer shifts of the two ions were assumed equal. In all the experimental and theoretical studies at sufficiently high temperature, typically at room temperature, only one average delocalized quadrupole doublet is observed.

In the present case, for **1** no broadening of the Mössbauer spectral lines is observed, and hence, we can confidently conclude that the electron detrapping occurs through vibronic coupling between charge localized and delocalized states. The Mössbauer spectra are of the "co-existence-type," as the localized and delocalized doublets are observed between 225 and 310 K with temperature dependent relative areas, see Figures 8, 10, 11, and 12. Hence, there must be two different relaxation rates, with two possible different origins, either fast tunneling between vibronic states and slow domain wall motion along the chain or fast and slow tunneling between the same and different iron 3d orbitals.

In the framework of the fast tunneling and slow domain wall motion model, we propose two explanations of the "coexistence" spectra. Because above 295 K the sum of the relative areas of the iron(II) and iron(III) doublets remains

---

(37) (a) Boukheddaden, J.; Linares, J.; Varret, F. *Phys. Rev. B* **1993**, *47*, 14070. (b) Boukheddaden, J.; Linares, J.; Varret, F. *Chem. Phys.* **1993**, *172*, 239.

(38) Varret, F.; Linares, J.; Boukheddaden, K. *J. Chem. Phys.* **1996**, *212*, 487.

(39) Linares, J.; Boukheddaden, J.; Varret, F. *Chem. Phys.* **1994**, *182*, 225.

constant at 50%, one is forced to conclude that in each tetrahedron of iron, when one pair of iron ions participates in the electron tunneling process, the other pair can not participate and is prohibited from undergoing the delocalization process, perhaps because the tunneling induces bond changes in the iron(II/III)−iron(II/III) bonding, see Figure 2. First, because the Fe1−Fe2 and Fe1*−Fe2* distances in Figure 1a are slightly different at 3.082 and 3.111 Å at 293 K, the doublet hyperfine parameters for the electron delocalization occurring between Fe1−Fe2 and Fe1*−Fe2* are slightly different. Second, if we assume that the same pair, for example, Fe1−Fe2, in all the tetrahedra, always participates in the tunneling process, then the other pair, for example, Fe1*−Fe2*, does not participate and contributes to the iron(II) and iron(III) doublets with 25% each of the spectral area. In the Fe1−Fe2 pair, each iron experiences average hyperfine parameters that are slightly different because the two iron sites are crystallographically inequivalent and contributes to two slightly different iron(II/III) doublets with 25% each of the spectral area. At this point, it is not possible to choose between these two explanations. However, the proposed transition at 275 K, see below, seems to favor the second explanation.

The coexistence of the iron(II), iron(III), and two iron(II/III) doublets between 225 and 320 K, with the temperature dependent relative areas shown in Figure 12, may be understood if there are domains along the $[Fe1^{II}_2(\mu_4\text{-O})\text{-}Fe2^{III}_2(\mu_4\text{-O})]^{6+}$ chains of **1** in which either fast tunneling occurs or fails to occur. These domains are separated by a domain wall that may also fluctuate. If the domain wall fluctuation rate is slow compared to the Mössbauer time scale, the Mössbauer spectrum will consist of the four narrow doublets with relative areas depending upon the relative volume fraction of the two different domains.

Now, the two-orbital vibronic coupling model developed for biferrocenium salts will be applied to the iron ions in **1**. In contrast with the biferrocenium salts, the iron ions in **1** are in the high-spin state and in a pseudooctahedral environment of oxygen ions. Hence, the iron(II) and iron(III) ions are expected to have the nominal $t_{2g}^4e_g^2$ and $t_{2g}^3e_g^2$ electronic configurations, with a crystal field splitting, $10D_q$, of the order of 10,000 cm^{-1} between the t_{2g} and e_g orbitals. Hence, it is highly unlikely that the electron detrapping process takes place between t_{2g} and e_g orbitals. Further, the tetragonal distortion of the octahedral environment of the iron ions will remove the degeneracy of the t_{2g} orbitals, as is indicated by the thermal dependence of the iron(II) quadrupole splitting, see Figure 11, and the corresponding low-symmetry splitting of the ground-state orbitals, t_{2g}, by 403 cm^{-1}. From the sign of the quadrupole splitting at the iron(II) in **1** we conclude that the d_{xz} and d_{yz} orbitals are either degenerate or close to degenerate and the d_{xy} orbital is at +403 cm^{-1}. Thus, we can propose that the orbitals involved in the orbital vibronic coupling are two of the t_{2g} orbitals, for example, the d_{xz} and the d_{yz} orbitals of the two iron ions. The temperature dependence of the iron(III) quadrupole splitting shown in Figure 11, that is, the slight tendency toward more positive values, see also Supporting Information, Table S2, between 225 and 310 K is also in agreement with this two-orbital vibronic relaxation model, a model that predicts that the two quadrupole splittings of the iron(II) and iron(III) doublets converge slightly and smoothly toward their average value.

The transition from the charge ordered to the charge disordered state seems to be second-order in view of the temperature dependence of the relative areas of the delocalized doublets, see Figure 12. Below 310 K, the completely delocalized state characterized by one average doublet is not observed. Hence, it appears that the relaxation rate between different d orbitals remains slow. It is, of course, possible that the completely delocalized state could be reached above 310 K; unfortunately, such studies are difficult because **1** is very susceptible to oxidative decomposition at higher temperature. It seems that perhaps **1** is exhibiting a partial transition or, alternatively it may exhibit a two-step transition with the second step above 310 K.

An Arrhenius plot of the equilibrium constant, that is, the delocalized to localized area ratio,[38] gives an entropy change of 151 J/K between 260 and 295 K. This values is about 17 times larger than the value of 9 J/K obtained in the biferrocenium diiodo bromide case[38] but is comparable with the entropy changes associated with the spin-state crossover processes. Hence, it seems that the order−disorder transition that takes place between 225 and 295 K is accompanied by subtle structural changes as is indicated in Figure 2. This large entropy change may also be associated with a first-order transition rather than a second-order transition.

As discussed above, the temperature dependence of the Mössbauer spectra may be understood in terms of two fluctuation rates, a fast tunneling rate for one electron and a slow fluctuation rate of the domain walls, separating the domains with and without the tunneling process, along the chain of **1**. Alternatively, the temperature dependence of the Mössbauer spectra may be understood at least in part in terms of a two-orbital vibronic relaxation model.[38] Whatever model is used, one question remains: Why is there a sudden increase in the tunneling rate beginning at about 260 K? The only reason must be the existence of a transition because in such a case the domains acquire their respective property immediately. This existence is further supported by the observation of a cusp in the temperature dependence of the magnetic susceptibility centered at about 275 K as is shown in the inset to Figure 3b. This transition could be either a first-order or a second-order transition. We'll first discuss the possibility of a first-order transition, a transition that is associated with a heterogeneous mixture of the high temperature domains with one electron delocalized between the iron(II)−iron(III) ions and the low temperature domains with no electron delocalization. The chains in **1** would thus consist of a mixture of very slow tunneling domains or segments and very fast tunneling domains or segments. If the first-order transition is not hysteretic, the coexistence of the four doublets between 225 and 320 K cannot be explained. However, if the first-order transition is hysteretic, the coexistence of the two phases with temperature dependent relative areas can result from domain growth kinetics. In the alternate two-orbital vibronic relaxation model, the existence of a first-order transition is possible in the presence a cooperative ligand field[39] and is supported by the large entropy change observed between 260 and 295 K.

At this point we do not know the order of the transition nor its hysteretic character, so the possibility of a second-order transition must be discussed. The temperature dependence of the relative areas of the iron(II) and iron(III) doublets shown in Figure 12 does, indeed, look like that of an order parameter for a second-order transition with a vertical slope at the critical temperature. However, the coexistence of the iron(II), iron(III), and iron(II/III) doublets is hard to explain in the absence of phase admixture. In the alternate two-orbital vibronic relaxation model, the existence of a second-order transition is possible, and the coexistence of the four doublets is predicted.

In conclusion, at this stage of the investigation of **1**, the existence of a transition centered at about 275 K can be proposed with confidence. This transition is observed both in the Mössbauer spectra and in the temperature dependence of the susceptibility. It is thus associated both with a change in the effective spin and the Curie constant. The small cusp observed at about 275 K in Figure 3b is associated with a non-magnetic transition that affects the magnetic properties. This transition is a charge order−disorder between a localized electron in a pair of iron(II)−iron(III) ions at low temperature and a delocalized electron yielding a pair of iron(II/III) ions at high temperature. This delocalization occurs through fast tunneling in domains whose size fluctuates slowly on the Mössbauer time scale or through vibronic coupling of two different orbitals on each iron ion of the pair. Both the order of the transition and the mechanism triggering it are undetermined at this time; however, the mechanism is likely to be related to the surprising changes in bond lengths shown in Figure 2.

Conclusions

The three-dimensional inorganic−organic hybrid $[Fe^{II}Fe^{III}(\mu_4\text{-O})(1,4\text{-chdc})_{1.5}]_\infty$, **1**, compound described herein features an unprecedented one-dimensional inorganic $[Fe^{II}_2(\mu_4\text{-O})Fe^{III}_2(\mu_4\text{-O})]^{6n+}$ mixed-spin and mixed-valence chain. This material exhibits a complex magnetic behavior including spin frustration in a one-dimensional ferrimagnetic chain above 36 K, interchain exchange interactions that lead to three-dimensional ferrimagnetic ordering below 32 K, and possibly relaxation dynamics of the spins between two different spin-canted magnetic structures or relaxation in a single-chain magnet below 22 K. In addition, as is clearly revealed by the Mössbauer spectral and magnetic suceptibility measurements, this material undergoes a charge order−disorder transition centered at about 275 K with the charge disorder state occurring through electron tunneling between the two minima in the energy surface or tunneling via vibronic coupling between two iron 3d orbitals.

Acknowledgment. The authors thank Dr. R. P. Hermann for many helpful and challenging discussions. This work was supported by the “973 Project” (2007CB815302), NSFC, No. 20821001, the Science and Technology Department of Guangdong Province, No. 04205405, and by the National Fund for Scientific Research, Belgium, Grant 1.5.064.05.

Supporting Information Available: CIF files, additional structural plots, additional magnetic plots, Mössbauer spectral parameters, and a powder X-ray diffraction pattern. This material is available free of charge via the Internet at http://pubs.acs.org.

IC8019155